Published in final edited form as:
Hippocampus. 2008 ; 18(4): 411–424. doi:10.1002/hipo.20404.

Distinct classes of pyramidal cells exhibit mutually exclusive firing patterns in hippocampal area CA3b

Peter Hemond[1], **Daniel Epstein**[1], **Angela Boley**[1], **Michele Migliore**[2], **Giorgio A. Ascoli**[3], and **David B. Jaffe**[1]

[1]Department of Biology, The University of Texas at San Antonio, One UTSA Circle, San Antonio, TX 78249

[2]Inst. of Biophysics, Nat. Res. Council, Palermo, Italy

[3]Krasnow Inst., George Mason Univ., Mail Stop 2A1, Fairfax, VA 22030

Abstract

It is thought that CA3 pyramidal neurons communicate mainly through bursts of spikes rather than so-called trains of regular firing action potentials. Reports of both burst firing and non-burst firing CA3 cells suggest that they may fire with more than one output pattern. With the use of whole-cell recording methods we studied the firing properties of rat hippocampal pyramidal neurons *in vitro* within the CA3b subregion and found three distinct types of firing patterns. Approximately 37% of cells were regular firing where spikes generated by minimal current injection (rheobase) were elicited with a short latency and with stronger current intensities trains of spikes exhibited spike frequency adaptation (SFA). Another 46% of neurons exhibited a delayed onset at rheobase with a weakly-adapting firing pattern upon stronger stimulation. The remaining 17% of cells showed a burst-firing pattern, though only elicited in response to strong current injection and spontaneous bursts were never observed. Control experiments indicated that the distinct firing patterns were not due to our particular slicing methods or recording techniques. Finally, computer modeling was used to identify how relative differences in K^+ conductances, specifically K_C, K_M, & K_D, between cells contribute to the different characteristics of the three types of firing patterns observed experimentally.

Keywords

action potential; adaptation; patch-clamp; bursting; potassium channel

Introduction

In awake behaving animals pyramidal neurons within the hippocampal formation fire action potentials over a wide range of frequencies and commonly spike in short high-frequency bursts (McNaughton *et al.*, 1983). During behavioral tasks the distribution of interspike intervals (ISI) of CA3 pyramidal neurons varies between cells (Frerking *et al.*, 2005) with

Corresponding author: David B. Jaffe, Ph.D. Department of Biology The University of Texas at San Antonio One UTSA Circle, San Antonio, TX 78249 Telephone: (210) 458 5843 Fax: (210) 458 5658 david.jaffe@utsa.edu.

some neurons exhibiting bimodal distributions suggestive of at least two firing patterns; burst firing which comprises a fast ISI peak and regular, lower-frequency firing corresponding to a longer ISI peak distribution (Frerking *et al.*, 2005).

CA3 pyramidal neurons *in vitro*, in contrast to CA1 pyramidal neurons (but see (Azouz et al., 1996; Golomb et al., 2006), are noted for exhibiting both spontaneous and evoked *intrinsic* burst firing; a brief high-frequency train of Na^+ spikes riding above a plateau potential (Bilkey and Schwartzkroin, 1990; Buckmaster and Amaral, 2001; Hablitz and Johnston, 1981; Johnston et al., 1980; Kole et al., 2004; Scharfman, 1993; Wong and Prince, 1978). Early studies suggested that a voltage-gated Ca^{2+} conductance is responsible for the inward current driving the plateau potential during a burst (Johnston et al., 1980; Wong and Prince, 1978), although a recent report suggests that slow persistent Na^+ channels may contribute to CA3 bursting in juvenile neurons (Sipila *et al.*, 2006).

That CA3 pyramidal neurons intrinsically burst-fire has formed the basis for a number of computational models of CA3 pyramidal neurons (Lazarewicz et al., 2002; Migliore et al., 1995; Traub et al., 1994; Traub et al., 1991) and the CA3 network (Menschik and Finkel, 1998; Staley et al., 2001; Traub et al., 1989; Yee et al., 2003). This circuit is of particular interest due to the strong recurrent excitation between pyramidal neurons (Johnston and Amaral, 1997) suggesting that it is an autoassociative network (Kohonen, 1977; McNaughton, 1989). Because of this circuitry it is also highly susceptible to epileptiform activity (Dzhala and Staley, 2003; Traub et al., 1987a; Yee et al., 2003). If the normal output mode of these cells is via bursts of action potentials, such firing patterns would have important computational implications for the CA3 circuit as well as its primary target, area CA1 (Lisman, 1997). Yet, there are also a number of reports where CA3 pyramidal neurons do not burst fire under conventional *in vitro* conditions (Major *et al.*, 1994; Saviane *et al.*, 2003; Young *et al.*, 2004) or that the occurrence of burst firing varies between cells (Bilkey and Schwartzkroin, 1990; Jensen and Yaari, 1997; Masukawa et al., 1982).

The morphology of CA3 pyramidal neurons varies along the distance of *s. pyramidale*; dendritic lengths increase in size with distance from the hilar region (Ishizuka et al., 1995) and so it is useful to divide area CA3 into three subregions, CA3a, b, & c (Lorente de Nó, 1934; Masukawa et al., 1982). Here we report that pyramidal neurons from within the medial portion of area CA3, the CA3b subfield—defined as the region within the fimbria and the blades of the dentate gyrus granule cell layer, can be divided into three different groups depending on their firing properties. We show that the variability in firing patterns, and the low frequency of finding of burst firing cells, was not due to methodological issues. Finally, a combination of experiments and computational modeling supports a working hypothesis that the three distinct firing patterns arise from cell-to-cell variability in membrane properties.

Materials and Methods

Hippocampal slices

Animal use was in accordance with the University of Texas at San Antonio University Institutional Animal Care and Use Committee. Sprague-Dawley rats (Harlan Sprague-

Dawley, Chicago, IL) 4-6 weeks old were first anesthetized with halothane and then followed by pentobarbital (130 mg/kg i.p.). Animals were perfused with an ice-cold (4 °C), oxygenated (95% O_2/5% CO_2) modified artificial cerebrospinal fluid (aCSF) containing (in mM): 124 choline chloride, 2.5 KCl, 26 $NaHCO_3$, 7 $MgCl_2$, 0.5 $CaCl_2$, 1.25 Na_2HPO_4, and 20 dextrose. Brains were removed and blocked to prepare horizontal brain slices (300-350 μm) containing transverse sections of the hippocampus with a vibratome (Vibratome Company, St. Louis, MO). Slices were first incubated for 30 minutes in a submerged holding chamber at 36-40 °C oxygenated with aCSF where choline chloride was replaced with equimolar NaCl. In addition, $CaCl_2$, $MgCl_2$, and dextrose were adjusted to 2-2.5, 1.3-2, and 10 mM, respectively. After this 30 minute period the tissue was allowed to return to room temperature (22-24 °C). Slices were transferred as needed to a submersion-type recording chamber mounted on an upright compound microscope (Zeiss Axioskop FS or Olympus BX50WI) perfused with oxygenated aCSF (~2 ml/min) at 34-35 °C. Except where noted excitatory and inhibitory synaptic transmission was blocked with kynurenate (1 mM) or CNQX (10 μM), APV (50 μM), and biccuculine (20 μM) added to the aCSF (Sigma-Aldrich, St. Louis, MO).

Patch-clamp Recording

Whole-cell and nystatin-patch recordings were made from pyramidal neurons in region CA3b. This area was operationally defined as the length of *s. pyramidale* that extended beyond the blades of the granule cell layer of the dentate gyrus to the fimbria (Masukawa et al., 1982). Cells were visually identified using infrared, video-DIC optics beneath a 40X water immersion objective. For whole-cell recording borosilicate glass pipettes (3-5 MΩ) were filled with either (in mM): 120 K-gluconate, 20 KCl, 2 $MgCl_2$, 0.1 ethylene glycol-bis[β-aminoethyl ether]-N,N,N',N'-tetraacetic acid (EGTA), 10 n-[2-Hydroxyethyl]piperazine-N'-2-ethanesulfonic acid (HEPES), 3 Na_2ATP, and 0.3 Na_2GTP or 140 $KMeSO_4$, 10 HEPES, 2 Na_2ATP, 0.4 Na_2GTP, and 2 $MgCl_2$. Experiments employing the $KMeSO_4$ pipette saline are noted. In some experiments, 0.5% biocytin was added to the saline. Series resistances were between 5-25 MΩ. For nystatin perforated patch recordings pipette tips were loaded with K-gluconate without nystatin (above) and backfilled with the same solution that included 500 μg/ml of nystatin (0.3% DMSO). Calculated liquid junction potentials for the K-gluconate and $KMeSO_4$ salines were +13.4 and +14.4 mV, respectively, and were not corrected.

Electrical recordings were made with an Axoclamp 2b (Axon Instruments, Foster City, CA) in bridge mode, filtered at 3-5 kHz, and digitized at 10-20 kHz with the use of an ITC-16 or ITC-18 interface (Instrutech, Great Neck, NY) connected to a Power Macintosh computer running custom software written with Igor Pro (Wavemetrics, Lake Oswego, OR).

Recordings made in the whole-cell configuration were taken after holding cells for approximately 15 minutes to allow for application of blockers (described above) and cells were typically held for between 10-45 minutes after that.

Biocytin-Fluorescent labeling

Where noted, a subset of cells were labeled with a fluorescein-avidin conjugate. Slices were fixed in paraformaldehyde (4%) and washed in a standard 0.1 M phosphate buffer solution (PBS). Slices were incubated in a 0.3% Triton-X PBS solution containing 2 μl/ml Fluorescein Avidin D (Vector Laboratories, Burlingame, CA) for 24 hours. Slices were then washed with PBS and visualized beneath a 10X water immersion objective on an Axioskop FS microscope equipped with epifluorescence illumination (488 nm excitation, 516 nm emission) using a cooled PXl-37 CCD camera (Photometrics, Tucson, AZ).

Extracellular Recording

Slices obtained as described above were placed in an interface chamber (34 °C) and perfused with aCSF (1 ml/min). Recording pipettes filled with 150 mM NaCl were placed in *stratum pyramidale* of area CA3b and a bipolar stimulus electrode was placed in the alveus to elicit antidromic responses. Stimulation consisted of a negative current pulse of 50 μs duration and current intensity ranging from 0-2 mA. Where noted, CNQX (10 μM), MK801 (40 μM), kynurenic acid (1 mM), and picrotoxin (50 μM) were added to the aCSF to block excitatory and inhibitory synaptic transmission.

Computer Modeling

All simulations were implemented using the NEURON simulation environment (v5.9, (Hines and Carnevale, 1997). In some cases, simulations were carried out using the *ParallelContext* class of NEURON on a 1024-processor IBM Linux cluster under MPI.

A 3D reconstruction, composed of 943 compartments, of a rat CA3b pyramidal neuron (*cell1zr*, downloaded from the public archive http://www.neuromorpho.org, (Ascoli, 2006) was used for all simulations. Uniform passive properties, consistent with the range of experimental values, were used for all simulations (τ_m = 35 ms, R_m = 25 kΩ·cm^2, R_a = 150 Ω·cm). The set of active dendritic properties included voltage-gated sodium (Na_V) conductances, a repertoire of potassium conductances including delayed rectifier (K_{DR}), KCNQ or M-current (K_M), fast-inactivating A-type (K_A), and slowly-inactivating D-type (K_D), three voltage-gated Ca^{2+} conductances (Ca_V N-, L- and T-type), two Ca^{2+}-dependent potassium conductances (K_C and K_{AHP}), and a hyperpolarization-activated conductance (I_h). Lastly, a simple Ca^{2+} extrusion mechanism (100 ms of decay time constant to a resting Ca^{2+} of 50 nM) was also included. Except for the K_D and the Ca^{2+} extrusion mechanism, all channels kinetics were very similar to those previously used to implement realistic CA1 (Na_V, K_{DR}, K_A, I_h, from Migliore, 2003; Migliore et al., 1999) or CA3 (Ca_V(N), Ca_V(L), Ca_V(T), K_M, K_C and K_{AHP}, from Migliore et al., 1995) pyramidal neurons. The voltage-dependence for inactivation for K_D was implemented as $n=1/(1+\alpha_n)$ and $\tau_n = 100\beta_n/(1+\alpha_n)$, with $\alpha_n = \exp(0.51\cdot(v+27))$, $\beta_n = \exp(0.36\cdot(v+27))$. We found that a +24mV shift of the Na_V, K_{DR}, K_M, and K_A activation and inactivation curves was needed to take into account the characteristics of experimentally-observed firing patterns. A more detailed explanation for this shift would require more information on the specific properties of each channel in these neurons. To the best of our knowledge this information is not currently available, and its investigation was well outside the purposes of this work. It should be stressed, however, that using this shift we were able to qualitatively model all the firing types without any

additional modifications of the channels properties. The complete model files are available for public download under the ModelDB section of the Senselab database (http://senselab.med.yale.edu).

The K_D and K_M channels were inserted only in the soma, whereas all the other channels were uniformly distributed over the entire dendritic arborization. A 100 μm long axon was connected to the model neuron. Conductances within the axon were limited to K_{DR}, K_A, along with a 5-fold increase in Na_V density in order to allow for axonal action potential initiation in response to somatic current injection. With these passive and active properties, the input resistance of the model was ~90MΩ.

In order to explore the extensive parameter space more efficiently, a reduced model of only one compartment was employed with the same passive membrane properties as the full model (C_m = 1.41 μF/cm^2, R_m = 25,000 Ωcm^2) and including all of the conductances, described above. Simulations were run with all possible combinations of these conductances with densities varied from 0, 0.25, 0.5, 1, 2, and 4 times values used for the full model and a range of input currents (0.01-0.3nA in steps of 0.02nA, for 400ms) for a total of 20,995,200 configurations. Four firing types were classified according to the following criteria: “bursting”: 4 spikes within the first 130ms; “adapting”: 6-8 spikes, first ISI < 100 ms, no subsequent ISI < 20 ms, ratio of any two consecutive ISIs < 0.8, and the ratio of the 6th-ISI/1st-ISI > 3; “non-adapting”: 5-8 spikes, the last-spike occurring > 200 ms after the start of the current step, and a ratio of any 2 consecutive ISIs in the range 0.9-1.1; “delayed”: 2-3 spikes generated by the current pulse and the first spike latency > 200ms. Additional rules were used to eliminate configurations resulting in a failure to fire or trapped in an inactivated state at the end of the current step.

Data analysis

Spike frequency adaptation (SFA) was quantified by plotting the interspike interval (ISI) versus the latency to the later of the two spikes. The slope of this plot could be fit by linear regression and the slope used as a measure of SFA. Comparisons between two groups were made with the use of a Student's t-test for paired samples (InStat, Graphpad Software, San Diego, CA). Smooth unimodal functions were obtained using the Gaussian curve fitting routine in IgorPro (Wavemetrics, Lake Oswego, OR) and compared to data using a Kolomogorov-Smirnov test.

Results

Spikes generated by minimal depolarization

To first test whether CA3 pyramidal neurons regularly burst fire or if there are more than one discrete forms of firing output, we started by examining the response to a minimal depolarizing current injection (rheobase) applied to the soma of CA3b pyramidal neurons (50-400 pA, 400 ms duration). Two examples of biocytin-filled CA3b pyramidal neurons are shown in Figure 1A. Where labeling was detected, all cells were pyramidal in appearance and localized within the cell body layer distal from *stratum lucidum* of area CA3b (n=13).

For all neurons single spikes were elicited with thresholds greater than 20 mV above the resting potential (Fig. 1B). Spontaneous firing was never observed in the presence of blockers of excitatory synaptic transmission. Resting potential for these cells was -60.5 ± 5.4 mV (n=43). The general characteristics of the action potential waveforms (Fig. 1B) were unremarkable and all within ranges previously described for hippocampal CA3 pyramidal neurons (half-width: 1.0 ± 0.1 ms; dV/dt: 101.6 ± 4.4 mV/ms; amplitude: 97.6 ± 1.9 mV; fast afterhyperpolarization, fAHP: 10.2 ± 0.5 mV; n=43). Cells with electrophysiological characteristics of inhibitory interneurons — large (>15 mV)/slower (>3 ms half-width) afterhyperpolariations and large input resistances (>300 MΩ) — were excluded from our analyses (Chitwood et al., 1999; Chitwood and Jaffe, 1998; Freund and Buzsaki, 1996).

Surprisingly, we found that there was a bimodal distribution for rheobase spike latency between cells (n=51). CA3 pyramidal cells either fired at the onset or fired toward the end of a 400 ms current step (Fig. 2A). The two modes of firing were clearly discernable. The best fit of a unimodal, Gaussian distribution of the entire data set had a mean of 55 ms (Fig. 2B). The difference between this unimodal distribution and the measured values was significantly different (Kolmogorov-Smirnov test; $D = 0.38$, $p < 0.05$). Late-firing cells, those neurons with latencies above the unimodal distribution described above (n=20) were best fit by Gaussian distribution with a mean of 340 ms. The mean latency for all 51 cells was 175 ± 135 milliseconds. For labeled cells (n=13) there was no obvious difference in the morphology between the two types of firing.

The occurrence of early- and late-onset groups of cells was not due to a systematic difference in the passive properties between cells. There was no correlation of membrane time constant (τ_m) or input resistance (R_N) with the rheobase spike latency (Fig. 2C). Mean values for τ_m and R_N were 61.4 ± 4.0 ms and 126 ± 8 MΩ , respectively (n=35), values were consistent with previous measurements of CA3 pyramidal neuron passive properties (Podlogar and Dietrich, 2006; Spruston and Johnston, 1992). Therefore, the differences in latency between the two groups of cells was not due to passive effects of slow membrane charging or steady-state potential. Likewise, we found no correlation between rheobase spike latency and resting potential, spike threshold, spike rise time, or spike half-width (Fig. 3).

Spike trains: Three firing patterns

To further test for variations in the excitability between CA3b pyramidal neurons, we next studied whether spike-frequency adaptation (SFA) was uniform between cells or was somehow correlated with the differences in rheobase spike latency, described above.

Stronger current steps (100-1500 pA), above rheobase, triggered trains of action potentials ranging up to 8-10 spike for a 400 ms pulse. We found that there was a large range of current amplitudes needed to obtain a relatively consistent number of spikes between cells. As expected, the magnitude of this current required to drive a train of spikes in any given cell was relatively proportional to its input resistance which varied 5-fold between cells (see Fig. 2C).

Three firing patterns were readily identified (Fig. 4A). At one extreme were those cells that exhibited a regular-firing pattern with strong SFA (quantified below). At the other were a second group of cells displaying weak to no SFA. Third and finally, there were cells that fired a rapid burst of spikes that rarely fired again during a current step. Each of these patterns was an intrinsic property of the cell and not due to recurrent synaptic regulation as both excitatory and inhibitory synaptic transmission was blocked. Intrinsic burst firing was operationally defined as a brief (< 100 ms) train of high-frequency (≥ 50 Hz) spikes produced by depolarizing current injection. These bursts of spikes were typically observed riding above a regenerative, plateau potential. It is also important to note that burst firing was never observed either spontaneously or in response to minimal current intensities.

To quantify and compare SFA we plotted the instantaneous spike interval (ISI) versus the latency of each interval from the onset of the current step (Fig. 4B). The slope of this relationship was used to quantitatively compare SFA between cells. ISI slope could range in these plots between 0-1, increasing with stronger SFA.

The distribution of ISI slopes varied uniformly within our data set from weak to strong adaptation (range: −0.03 to 0.80, mean 0.34 ± 0.04, n = 43). Burst firing cells all fired a single spike with an early onset in response to a minimal current injection (rheobase). When all early-firing cells were combined, burst firing cells were identified as those cells that fell outside of a unimodal distribution of mean firing rate (≥ 50 Hz) (Fig. 4C). Burst firing cells had a mean ISI slope of 0.36 ± 0.06 and a mean frequency of 82 ± 0.06 Hz (n=7).

We noticed that early-onset cells tended to have stronger SFA. To quantify this observation the ISI slope of non-bursting cells was plotted against rheobase spike latency for each cell (Fig. 4D). There was a significant correlation between the onset of rheobase spikes and the magnitude of SFA ($r^2 = 0.32$, $p < 0.05$; Pearson product-moment correlation test); late-onset cells were more likely to exhibit weaker SFA compared with early-onset cells that exhibited stronger SFA. Overall, regular-firing cells comprised 37% of the data set, while weakly-adapting neurons were found in 46% of our neurons. The remaining 16% of cells were classified as burst firing (described further below). It is important to point out that all cells were obtained from different slices. Where data was obtained in a series of cells from the same animal (2-3 neurons per animal) no consistent firing pattern was observed. Finally, it is important to point out that membrane responses and firing patterns were stable throughout the course of each experiment.

Slowly-inactivating K^+ conductance delays rheobase spikes

We hypothesized that the expression of a slowly-inactivating K^+ conductance (K_D) in a subset of cells could lead to delayed onset of rheobase spikes and might counter other conductances contributing to SFA. To test this hypothesis, low concentrations (< 50 μM) of 4-aminopyridine (4-AP) was used to block K_D (Mitterdorfer and Bean, 2002). For late-onset cells, bath application of 4-AP (30 μM) increased excitability (Fig. 5A). For late-firing, weakly-adapting neurons there was a significant reduction in rheobase spike latency (t=11.3, df=3, p<0.01). This was accompanied by decreases in rheobase current, an increase spike number, and an increase in SFA as indicated by the ISI slope (Fig. 5B). In contrast, for

early-onset neurons the same concentration of 4-AP had no significant effect on the latency of rheobase spikes or SFA (Fig. 5B).

A small proportion of burst firing CA3b neurons

As mentioned above, the occurrence of burst firing cells was less than 20%. In these cells, when more than two spikes were elicited a brief (<100 ms) high-frequency (50-100 Hz) spike trains was observed riding above a plateau potential (Fig. 6A). In contrast, rheobase current elicited only a single early-onset spike and never triggered a burst of spikes. The inability of CA3b pyramidal neurons to routinely burst fire was not due to slice conditions. Burst firing pyramidal neurons were found in the subiculum (Jung *et al.*, 2001) and, moreover, in the same slice of tissue where we could find burst firing cells in the subiculum, CA3b neurons still failed to produce bursts of spikes (Fig. 6B).

Extracellular K^+ concentration was not a factor limiting the our cells from exhibiting intrinsic burst firing behavior (Jensen and Yaari, 1997). Increasing extracellular concentration to 5 mM depressed both fast and medium AHPs (n=10), thus enhancing excitability, but did not expose burst firing for short, lower intensity pulses (Fig. 6C). In these same experiments when membrane potential was hyperpolarized to −80 and −90 mV, in an attempt to de-inactivate low-threshold voltage-gated Ca^{2+} channels or slow Na^+ channels, burst firing was still not achieved. That said, only when depolarizing pulses were longer or and increased in amplitude were we were able to elicit a burst-like firing pattern with 5 mM extracellular K^+ (Fig. 6D).

We tested whether depolarized CA3 pyramidal neurons would burst fire without perturbing the cell with intracellular recording methods. Here we recorded extracellular population field potentials from area CA3b in response to antidromic stimulation of *s. oriens*, within 1 mm of the recording electrode (Fig. 6D). These experiemnts were performed in the presence of blockers of excitatory and inhibitory synaptic transmission to prevent repetitive firing produced by recurrent excitation. In all cases (n=7) over a range of stimulus intensities the response was dominated by a single population spike (PS). Although second-order population events appeared at the strongest stimulus intensities, their amplitude was less than 20% of the first PS amplitude indicating that, for the majority of cells, antidromic stimulation triggered only a single action potential and not a burst of spikes.

An additional set of experiments were also performed using the perforated-patch method. Both early-onset/adapting and late-onset/weakly-adapting CA3b pyramidal neurons were observed with nystatin-patch recordings (Fig. 7). Out of six neurons studied four were characterized as early-onset/adapting and two were late-onset/weakly-adapting. Burst firing was not observed for any cells recorded with perforated-patch. Finally, we found no significant difference in the characteristics of individual spikes between whole-cell and perforated patch recordings.

Firing patterns in response to more physiologically-relevant stimuli

Rectangular depolarizing current steps, as employed above, are widely used to characterize the firing properties of neurons. To better characterize the response of CA3b pyramidal

neurons to what would more approximate physiological stimulus of the cell, that is synaptic input over time, and to test the hypothesis that burst firing might arise from such membrane fluctuations, we examined firing patterns produced by a model of synaptic bombardment where a "noisy" injected current was applied to the soma. The waveform was generated by convolving white noise over a filtering frequency as previously described (Mainen and Sejnowski, 1995).

A series of 15 rectangular current steps was first applied with an amplitude that typically elicited 3-4 spikes (Fig. 8A). Note that in these particular experiments, a $KMeSO_4$ pipette saline was used and no blockers were added to the bathing medium. Nevertheless, we still observed with rectangular depolarizing current steps the heterogeneity of firing patterns described above. As expected, the reliability of spike timing was variable between trials, especially those occurring in the later two-thirds of the trial. In contrast, when current was injected in the form of a noisy signal repeated sequentially, where the mean current was equal to the amplitude of a rectangular current step (equivalent total charge), firing was highly reliable across trials; spikes occurred at the same regular intervals for each trail (Mainen and Sejnowski, 1995). Overall, no significant differences in reliability were discerned between early-/adapting and late-onset/weakly-adapting cells, or for burst firing cells where the current amplitude was subthreshold for the burst.

In no cases was burst firing elicited for regularly-firing or weakly-adapting cells in response to the noisy input. Additionally, we found that for all cells the noisy current stimulus was more effective at generating spikes than a rectangular current step (Fig. 8B). For all types of cells (early-/adapting, late-onset/weakly-adapting, and burst firing) the mean number of spikes generated by a noisy input was 2.5-fold more than for rectangular current injection ($t=3.94$, $df=9$, $p < 0.01$).

Computational models of distinct firing patterns

To examine how individual ionic conductances might contribute to the various firing patterns, we first constructed a model using a reconstruction of a CA3 pyramidal neuron (Henze *et al.*, 1996), a repertoire of somatic and dendritic voltage-dependent ion channels, and intracellular calcium dynamics (Fig. 9A, see Methods). Conductance densities were initially adjusted to generate a model with a spike threshold ~20 mV above V_{rest} and where burst firing was elicited at suprathreshold current intensities well above rheobase (Fig. 9B; see also Fig. 4A).

We used the model to determine what minimal changes in membrane conductances might be needed to transform the firing patterns between early-/adapting, late-onset/weakly-adapting, and burst firing. Burst firing in the model was dependent on relative densities of the Ca^{2+}-dependent K^+ and delayed rectifier K^+ conductances, K_C & K_{DR}, respectively. Eliminating K_C and raising K_{DR} approximately 2-fold converted the burst- firing model to one that exhibited adaptation (Fig. 9C). Burst firing in this model was therefore contingent upon the presence of K_C acting to terminate the burst, while enhancing K_{DR} was needed to compensate for the loss of total outward current.

Adaptation in the model was dependent on a slowly-activating K^+ conductance, K_M. Reducing this conductance converted a strongly adapting firing pattern to one that lacked SFA (Fig. 9D). Interestingly, lowering a slow Ca^{2+}-dependent K^+ conductance, K_{AHP}, had little effect on adaptation such that that K_M primarily mediated SFA (simulation not shown). Finally, to achieve delayed onset firing inclusion of a slowly-inactivating K^+ conductance, K_D, was required for the model (Fig. 9E). This is consistent with our experimental observation that blocking K_D transforms late-onset into early-onset CA3b pyramidal neurons (see Fig. 5).

To understand better how various repertoires of voltage-gated conductances contributed to the different firing patterns we employed a single-compartment model containing the eight voltage-gated conductances, using a brute force approach to explore the parameter space. This has been a useful approach to investigate the parameter space for both single-compartment (Prinz et al., 2003) and small network models (Prinz et al., 2004), demonstrating that even using a coarse grid of conductance values it is possible to capture all the main firing properties of a small system. To understand better how various repertoires of voltage-gated conductances contributed to the different firing patterns and to further explore the parameter space, we employed a single compartment model containing the eight voltage-gated conductances. We varied each conductance by 0, 0.25, 0.5, 1, 2, and 4 times values from the multicompartmental model and, in addition, varied stimulus current between 0.1-0.3 nA at 0.02 nA steps (duration 400 ms) for a total of 20,995,200 different configurations. Of these, only 91,914 configurations (0.4%) fired spikes and returned to a resting potential allowing for classification within any one of four types of firing patterns (see Methods; Fig. 10A). Of these remaining configurations, 94% exhibited a burst-firing pattern, while the remaining patterns were as follows: 2% adapting, 3% non-adapting, and 1% a delayed firing pattern.

In Figure 10B the relative conductances requires on average to achieve each of the four patterns are plotted. Three important observations can be made from these plots. First, for configurations resulting in a burst-firing pattern, there were on average larger densities of 4 of the 6 outward currents (K_C, K_{DR}, K_A, and K_M) with concomitant increases in g_{Na} and g_{Ca}. The ratio of outward to inward currents was the largest for burst-firing models suggesting that the specific increases in K_C, K_{DR}, and K_A permits higher spiking rates during the burst and greater K_M (but not K_{AHP}) shuts it down. Second, delayed onset required an increase in K_D. For these two firing patterns (burst and delayed), it appears that increases in outward currents are followed by the inward currents as well. This is further illustrated in Figure 10C comparing the relative total outward and inward currents between configurations resulting in the different firing patterns. Third, the average magnitudes of the conductances required for adapting and non-adapting cells are comparable except for K_M which was nearly 3 times larger for achieving an adapting firing pattern, whereas the slow AHP conductance had little effect. Finally, the type of firing pattern expressed by a configuration was not affected by variations in passive properties. As mentioned above, the membrane time constant and input resistance could vary 5-fold between cells (Fig. 2C). Increasing membrane resistivity, with a comparable decrease in stimulus current to maintain the same spike number, had no effect on the firing pattern produced by a particular configuration of the model (not shown). The reason for this effect is that, in contrast with

past studies, bursting behavior here was not dependent on the appropriate coupling between a fast sodium (somatic) signal with a slower calcium (dendritic) dynamics (Pinsky and Rinzel, 1994). Rather, we find that burst-firing may also simply result from specific combinations of inward and outward currents.

Discussion

In this study we examined the firing properties of pyramidal neurons in the CA3b subregion of the hippocampal formation *in vitro*. Our primary finding is that intrinsic burst firing was not the primary mode of output for these cells under normal *in vitro* conditions, but that three distinct firing patterns were observed; i) a regular firing pattern where there was a short latency to a spike elicited by a minimal somatic current (rheobase) and with stronger stimuli there was robust SFA, ii) a weakly-adapting pattern where rheobase current triggered a spike after a significantly longer delay, while with stronger depolarizing current injection there was little SFA, and iii) a burst-firing pattern where rheobase current triggered a single spike with a short latency, but with stronger stimuli a brief burst of high-frequency spikes was elicited.

The low occurrence and the high-threshold of burst firing pyramidal neurons was a surprise. Based on previous work going back more than 20 years, we expected most pyramidal neurons to burst fire both spontaneously and in response to modest depolarizing current stimuli (Buckmaster and Amaral, 2001; Hablitz and Johnston, 1981; Johnston et al., 1980; Kole et al., 2004; Traub et al., 1987a; Traub et al., 1987b). Neither was the case; spontaneous burst firing was never observed and only single spikes were observed at rheobase current amplitudes.

It is difficult to reconcile our observations with the possibility that a lack of burst firing is due to methodological considerations (Major *et al.*, 1994; Saviane *et al.*, 2003; Young *et al.*, 2004). First, we could find burst firing neurons in the subiculum (Jung et al., 2001; Staff et al., 2000), while within the same slice of tissue CA3b pyramidal neurons failed to burst-fire. That said, we cannot rule out the possibility that differences between slices might contribute to the properties of CA3 pyramidal neurons. At the same time, where data was obtained from the same animal in a series of cells on a given day there was no consistent firing pattern suggesting that the state of the animals used in this study was not a factor (but see Kole et al., 2001). Second, we tested whether excitability was affected by extracellular K^+ concentration (Jensen and Yaari, 1997). Burst firing could only be elicited when stimulus strength was of a sufficient duration and strength; rheobase stimulation generated only a single spike. The higher threshold for eliciting a burst under these conditions may suggest that the source of the regenerative event is distal from the soma. It is important to point out that extracellular K^+ *in vivo* is normally 2-3.5 mM (Jones and Keep, 1987; Moghaddam and Adams, 1987) and raising extracellular K^+ concentration to 5 mM is a robust way of generating epileptiform activity in hippocampal slices (Korn et al., 1987; Rutecki et al., 1985; Swartzwelder et al., 1986). Third, we controlled for the effects of intracellular dialysis from whole-cell pipettes with experiments employing perforated patch-clamp recording. Fourth, and finally, in extracellular recordings from slices maintained in an interface chamber (as opposed to a submerged chamber used for our intracellular recordings) we

found that antidromically-stimulated CA3 pyramidal neurons–under conditions where both excitatory and inhibitory synaptic transmission were blocked–also did not burst fire as a population. Therefore, burst firing is not contingent on the recording conditions (submerged versus interface slices) or on any possible perturbations inflicted by any type of intracellular recording method (sharp versus whole-cell versus perforated patch).

It is possible that one or more extrinsic factors such as stress levels of the animal or other such determinants may affect CA3 pyramidal neuron excitability (Ko*le et al., 2*001). It is also quite possible that excitability varies with subfield location, such as between areas CA3a-c or across dorsal to ventral hippocampus. Indeed, our results are most consistent with the sharp-electrode study of Masukawa et al. (1982) where they found that the occurrence of burst firing cells dropped from 60% in CA3a to 10% in CA3b. In contrast, Bilkey and Schwartzkroin (1990) recording from pyramidal cells from CA3a-c, generally found that the occurrence of burst firing cells (80% of the cells) was correlated with the location of the soma lying at the edge of the pyramidal cell layer, which we did not observe.

Our results point to heterogeneity of CA3b pyramidal neurons in at least two domains. First, the passive properties of these cells varies almost 10-fold suggesting a continuum of integrative function from low to high R_N & τ_m cells (Spruston and Johnston, 1992). Second, CA3b pyramidal neurons *in vitro* could be divided by three distinct firing patterns; adapting (regular firing), weakly adapting, and burst firing (Fig. 3C). The firing pattern of the regularly firing cells appears qualitatively similar to that of a canonical non-burst firing CA1 pyramidal neuron (Jensen and Yaari, 1997), while those of burst firing and weak-adapting cells do not. In particular, the weak-adapting cells appear to have at least two characteristic features; a mechanism that delays the onset of spikes produced by minimal input, possibly by greater expression of a slowly-inactivating K^+ conductance (Saviane et al., 2003), and an attenuated mechanism of adaptation which may result from reduced K_M or slow Ca^{2+}-dependent potassium conductances.

The present study also points to an alternative view of burst firing in CA3 pyramidal neurons. For most previous models of CA3 pyramidal neurons burst firing was, in most cases, an all-or-none event (but see Scharfman, 1993) mediated either by voltage-activated Ca^{2+} channels (Hablitz and Johnston, 1981; Johnston et al., 1980; Lazarewicz et al., 2002; Migliore et al., 1995; Traub et al., 1994) or persistent Na^+ conductances (Sipila *et al.*, 2006). In contrast, burst firing cells in our hands, besides being harder to find, were high-threshold events requiring relatively strong depolarizing current amplitudes (see also Azouz et al., 1997).

There are computational advantages for a cell to burst-fire (Lisman, 1997) and it is well established that hippocampal pyramidal neurons can fire in bursts *in vivo*; brief episodes of high-frequency firing, as observed in single unit records, are generally referred to as “complex spikes” (McNaughton *et al.*, 1983), though this type of output may represent one portion of a continuum of firing patterns (Harris et al., 2001).

Our brute-force survey of parameter space identified a much greater, more robust range of voltage-gated conductances that produced burst-firing, in contrast to the repertoire of

channels needed to “tune” the model to a non-burst firing pattern. Prinz and Marder first employed such an approach to simulations of spontaneously burst-firing stomatogastric neurons (Prinz et al., 2003). As in that study, the advantage is not only in the finding the optimal parameters, but also the insight gained from how different conductances co-vary between subtle and not-so-subtle differences in the models’ output. Here, it was the unexpected greater density of outward currents, presumably needed for high-frequency firing during the burst (Erisir et al., 1999), in addition to the expected drive of inward currents (Johnston et al., 1980; Pinsky and Rinzel, 1994), consistently expressed across parameters that produced burst-firing.

A regenerative burst of spikes, as observed in intracellular recordings, is by definition an all-or-none event and the number of spikes produced by a given somatic stimulus is relatively constant (Lazarewicz et al., 2002; Migliore et al., 1995). It may be advantageous, computationally, for the network to have a diverse populations of neurons ranging from those cells that are non-bursting firing (lower gain) to those that do exhibit a burst of spikes for a relatively equivalent input (higher gain), with varying amounts of adaptation in between.

CA3 pyramidal neurons *in vivo* exhibit a range of firing patterns that can be interpreted as spanning from non-bursting to burst firing (Frerking et al., 2005). It is quite possible that the variability we observed *in vitro* contributes, at least in part, to that distribution. It is also quite possible that complex spikes *in vivo* (i.e. burst firing) may be more controlled by synaptic (network) drive rather than simply a given neuron's intrinsic excitability. This hypothesis is supported by the fact that complex spikes can be observed in area CA1 *in vivo* (Harris et al., 2001; McNaughton et al., 1983) in spite of the general view that CA1 pyramidal neurons *in vitro* are not burst firing cells (but see (Azouz et al., 1996; Golomb et al., 2006). Furthermore, the close regulation of burst-firing is supported by evidence that it is contingent on behavior (Tropp Sneider *et al.*, 2006), suggesting an interplay between the intrinsic properties of the cell and synaptic drive.

Acknowledgements

This work was supported by CRCNS grant AG25633. We thank Drs. German Barrionuevo and Helen Scharfman for helpful comments on an earlier version of this manuscript. We also thank the CINECA consortium (Bologna, Italy) for granting access to their multiprocessor systems.

References

Ascoli GA. Mobilizing the base of neuroscience data: the case of neuronal morphologies. Nat Rev Neurosci. 2006; 7:318–24. [PubMed: 16552417]

Azouz R, Alroy G, Yaari Y. Modulation of endogenous firing patterns by osmolarity in rat hippocampal neurones. J Physiol. 1997; 502(Pt 1):175–87. [PubMed: 9234205]

Azouz R, Jensen MS, Yaari Y. Ionic basis of spike after-depolarization and burst generation in adult rat hippocampal CA1 pyramidal cells. J Physiol. 1996; 492(Pt 1):211–23. [PubMed: 8730596]

Bilkey DK, Schwartzkroin PA. Variation in electrophysiology and morphology of hippocampal CA3 pyramidal cells. Brain Res. 1990; 514:77–83. [PubMed: 2357533]

Buckmaster PS, Amaral DG. Intracellular recording and labeling of mossy cells and proximal CA3 pyramidal cells in macaque monkeys. J Comp Neurol. 2001; 430:264–81. [PubMed: 11135261]

Chitwood RA, Hubbard A, Jaffe DB. Passive electrotonic properties of rat hippocampal CA3 interneurones. J Physiol. 1999; 515:743–56. [PubMed: 10066901]

Chitwood RA, Jaffe DB. Calcium-dependent spike-frequency accommodation in hippocampal CA3 nonpyramidal neurons. J Neurophysiol. 1998; 80:983–8. [PubMed: 9705484]

Dzhala VI, Staley KJ. Transition from interictal to ictal activity in limbic networks in vitro. J Neurosci. 2003; 23:7873–80. [PubMed: 12944517]

Erisir A, Lau D, Rudy B, Leonard CS. Function of specific K(+) channels in sustained high-frequency firing of fast-spiking neocortical interneurons. J Neurophysiol. 1999; 82:2476–89. [PubMed: 10561420]

Frerking M, Schulte J, Wiebe SP, Staubli U. Spike timing in CA3 pyramidal cells during behavior: implications for synaptic transmission. J Neurophysiol. 2005; 94:1528–40. [PubMed: 15872069]

Freund TF, Buzsaki G. Interneurons of the hippocampus. Hippocampus. 1996; 6:347–470. [PubMed: 8915675]

Golomb D, Yue C, Yaari Y. Contribution of persistent Na+ current and M-type K+ current to somatic bursting in CA1 pyramidal cells: combined experimental and modeling study. J Neurophysiol. 2006; 96:1912–26. [PubMed: 16807352]

Hablitz JJ, Johnston D. Endogenous nature of spontaneous bursting in hippocampal pyramidal neurons. Cell Mol Neurobiol. 1981; 1:325–34. [PubMed: 6765736]

Harris KD, Hirase H, Leinekugel X, Henze DA, Buzsaki G. Temporal interaction between single spikes and complex spike bursts in hippocampal pyramidal cells. Neuron. 2001; 32:141–9. [PubMed: 11604145]

Henze DA, Cameron WE, Barrionuevo G. Dendritic morphology and its effects on the amplitude and rise-time of synaptic signals in hippocampal CA3 pyramidal cells. J Comp Neurol. 1996; 369:331–44. [PubMed: 8743416]

Hines ML, Carnevale NT. The NEURON simulation environment. Neural Comput. 1997; 9:1179–209. [PubMed: 9248061]

Ishizuka N, Cowan WM, Amaral DG. A quantitative analysis of the dendritic organization of pyramidal cells in the rat hippocampus. J Comp Neurol. 1995; 362:17–45. [PubMed: 8576427]

Jensen MS, Yaari Y. Role of intrinsic burst firing, potassium accumulation, and electrical coupling in the elevated potassium model of hippocampal epilepsy. J Neurophysiol. 1997; 77:1224–33. [PubMed: 9084592]

Johnston, D.; Amaral, D. Hippocampus.. In: Shepherd, GM., editor. The synaptic organization of the brain. Oxford University; New York: 1997.

Johnston D, Hablitz JJ, Wilson WA. Voltage clamp discloses slow inward current in hippocampal burst-firing neurones. Nature. 1980; 286:391–3. [PubMed: 7402320]

Jones HC, Keep RF. The control of potassium concentration in the cerebrospinal fluid and brain interstitial fluid of developing rats. J Physiol. 1987; 383:441–53. [PubMed: 3656129]

Jung HY, Staff NP, Spruston N. Action potential bursting in subicular pyramidal neurons is driven by a calcium tail current. J Neurosci. 2001; 21:3312–21. [PubMed: 11331360]

Kohonen, T. Associative memory: A system theoretic approach. Springer-Verlag; 1977.

Kole MH, Czeh B, Fuchs E. Homeostatic maintenance in excitability of tree shrew hippocampal CA3 pyramidal neurons after chronic stress. Hippocampus. 2004; 14:742–51. [PubMed: 15318332]

Kole MH, Koolhaas JM, Luiten PG, Fuchs E. High-voltage-activated Ca2+ currents and the excitability of pyramidal neurons in the hippocampal CA3 subfield in rats depend on corticosterone and time of day. Neurosci Lett. 2001; 307:53–6. [PubMed: 11516573]

Korn SJ, Giacchino JL, Chamberlin NL, Dingledine R. Epileptiform burst activity induced by potassium in the hippocampus and its regulation by GABA-mediated inhibition. J Neurophysiol. 1987; 57:325–40. [PubMed: 3559679]

Lazarewicz MT, Migliore M, Ascoli GA. A new bursting model of CA3 pyramidal cell physiology suggests multiple locations for spike initiation. Biosystems. 2002; 67:129–37. [PubMed: 12459292]

Lisman JE. Bursts as a unit of neural information: making unreliable synapses reliable. Trends Neurosci. 1997; 20:38–43. [PubMed: 9004418]

Lorente de Nó R. Studies on the structure of the cerebral cortex. II. Continuation of the study of the ammonic system. J. Psychol. Neurol. 1934; 46:113–177.

Mainen ZF, Sejnowski TJ. Reliability of spike timing in neocortical neurons. Science. 1995; 268:1503–6. [PubMed: 7770778]

Major G, Larkman AU, Jonas P, Sakmann B, Jack JJ. Detailed passive cable models of whole-cell recorded CA3 pyramidal neurons in rat hippocampal slices. J Neurosci. 1994; 14:4613–38. [PubMed: 8046439]

Masukawa LM, Benardo LS, Prince DA. Variations in electrophysiological properties of hippocampal neurons in different subfields. Brain Res. 1982; 242:341–4. [PubMed: 7116139]

McNaughton, BL. Neuronal mechanisms for spatial computation and information storage.. In: Nadel, L.; Cooper, LA.; Pulicover, P.; Harnish, RM., editors. Neural Connections. MIT Press; Mental Computation. London: 1989.

McNaughton BL, Barnes CA, O'Keefe J. The contributions of position, direction, and velocity to single unit activity in the hippocampus of freely-moving rats. Exp Brain Res. 1983; 52:41–9. [PubMed: 6628596]

Menschik ED, Finkel LH. Neuromodulatory control of hippocampal function: towards a model of Alzheimer's disease. Artif Intell Med. 1998; 13:99–121. [PubMed: 9654381]

Migliore M. On the Integration of Subthreshold Inputs from Perforant Path and Schaffer Collaterals in Hippocampal CA1 Pyramidal Neurons. J Comput Neurosci. 2003; 14:185–192. [PubMed: 12567016]

Migliore M, Cook EP, Jaffe DB, Turner DA, Johnston D. Computer simulations of morphologically reconstructed CA3 hippocampal neurons. J Neurophysiol. 1995; 73:1157–68. [PubMed: 7608762]

Migliore M, Hoffman DA, Magee JC, Johnston D. Role of an A-type K+ conductance in the back-propagation of action potentials in the dendrites of hippocampal pyramidal neurons. J Comput Neurosci. 1999; 7:5–15. [PubMed: 10481998]

Mitterdorfer J, Bean BP. Potassium currents during the action potential of hippocampal CA3 neurons. J Neurosci. 2002; 22:10106–15. [PubMed: 12451111]

Moghaddam B, Adams RN. Regional differences in resting extracellular potassium levels of rat brain. Brain Res. 1987; 406:337–40. [PubMed: 3567631]

Pinsky PF, Rinzel J. Intrinsic and network rhythmogenesis in a reduced Traub model for CA3 neurons. J Comput Neurosci. 1994; 1:39–60. [PubMed: 8792224]

Podlogar M, Dietrich D. Firing pattern of rat hippocampal neurons: a perforated patch clamp study. Brain Res. 2006; 1085:95–101. [PubMed: 16584711]

Prinz AA, Billimoria CP, Marder E. Alternative to hand-tuning conductance-based models: construction and analysis of databases of model neurons. J Neurophysiol. 2003; 90:3998–4015. [PubMed: 12944532]

Prinz AA, Bucher D, Marder E. Similar network activity from disparate circuit parameters. Nat Neurosci. 2004; 7:1345–52. [PubMed: 15558066]

Rutecki PA, Lebeda FJ, Johnston D. Epileptiform activity induced by changes in extracellular potassium in hippocampus. J Neurophysiol. 1985; 54:1363–74. [PubMed: 2416891]

Saviane C, Mohajerani MH, Cherubini E. An ID-like current that is downregulated by Ca2+ modulates information coding at CA3-CA3 synapses in the rat hippocampus. J Physiol. 2003; 552:513–24. [PubMed: 14561833]

Scharfman HE. Spiny neurons of area CA3c in rat hippocampal slices have similar electrophysiological characteristics and synaptic responses despite morphological variation. Hippocampus. 1993; 3:9–28. [PubMed: 8364685]

Sipila ST, Huttu K, Voipio J, Kaila K. Intrinsic bursting of immature CA3 pyramidal neurons and consequent giant depolarizing potentials are driven by a persistent Na+ current and terminated by a slow Ca2+ -activated K+ current. Eur J Neurosci. 2006; 23:2330–8. [PubMed: 16706841]

Spruston N, Johnston D. Perforated patch-clamp analysis of the passive membrane properties of three classes of hippocampal neurons. J Neurophysiol. 1992; 67:508–29. [PubMed: 1578242]

Staff NP, Jung HY, Thiagarajan T, Yao M, Spruston N. Resting and active properties of pyramidal neurons in subiculum and CA1 of rat hippocampus. J Neurophysiol. 2000; 84:2398–408. [PubMed: 11067982]

Staley KJ, Bains JS, Yee A, Hellier J, Longacher JM. Statistical model relating CA3 burst probability to recovery from burst-induced depression at recurrent collateral synapses. J Neurophysiol. 2001; 86:2736–47. [PubMed: 11731533]

Swartzwelder HS, Sutch CP, Wilson WA. Attenuation of epileptiform bursting by baclofen: reduced potency in elevated potassium. Exp Neurol. 1986; 94:726–34. [PubMed: 3780917]

Traub RD, Jefferys JG, Miles R, Whittington MA, Toth K. A branching dendritic model of a rodent CA3 pyramidal neurone. J Physiol. 1994; 481(Pt 1):79–95. [PubMed: 7853251]

Traub RD, Knowles WD, Miles R, Wong RK. Models of the cellular mechanism underlying propagation of epileptiform activity in the CA2-CA3 region of the hippocampal slice. Neuroscience. 1987a; 21:457–70. [PubMed: 3039403]

Traub RD, Miles R, Wong RK. Model of the origin of rhythmic population oscillations in the hippocampal slice. Science. 1989; 243:1319–25. [PubMed: 2646715]

Traub RD, Miles R, Wong RK, Schulman LS, Schneiderman JH. Models of synchronized hippocampal bursts in the presence of inhibition. II. Ongoing spontaneous population events. J Neurophysiol. 1987b; 58:752–64. [PubMed: 3681393]

Traub RD, Wong RK, Miles R, Michelson H. A model of a CA3 hippocampal pyramidal neuron incorporating voltage-clamp data on intrinsic conductances. J Neurophysiol. 1991; 66:635–50. [PubMed: 1663538]

Tropp Sneider J, Chrobak JJ, Quirk MC, Oler JA, Markus EJ. Differential behavioral state-dependence in the burst properties of CA3 and CA1 neurons. Neuroscience. 2006; 141:1665–77. [PubMed: 16843607]

Wong RK, Prince DA. Participation of calcium spikes during intrinsic burst firing in hippocampal neurons. Brain Res. 1978; 159:385–90. [PubMed: 728808]

Yee AS, Longacher JM, Staley KJ. Convulsant and anticonvulsant effects on spontaneous CA3 population bursts. J Neurophysiol. 2003; 89:427–41. [PubMed: 12522191]

Young SR, Chuang SC, Wong RK. Modulation of afterpotentials and firing pattern in guinea pig CA3 neurones by group I metabotropic glutamate receptors. J Physiol. 2004; 554:371–85. [PubMed: 14578486]

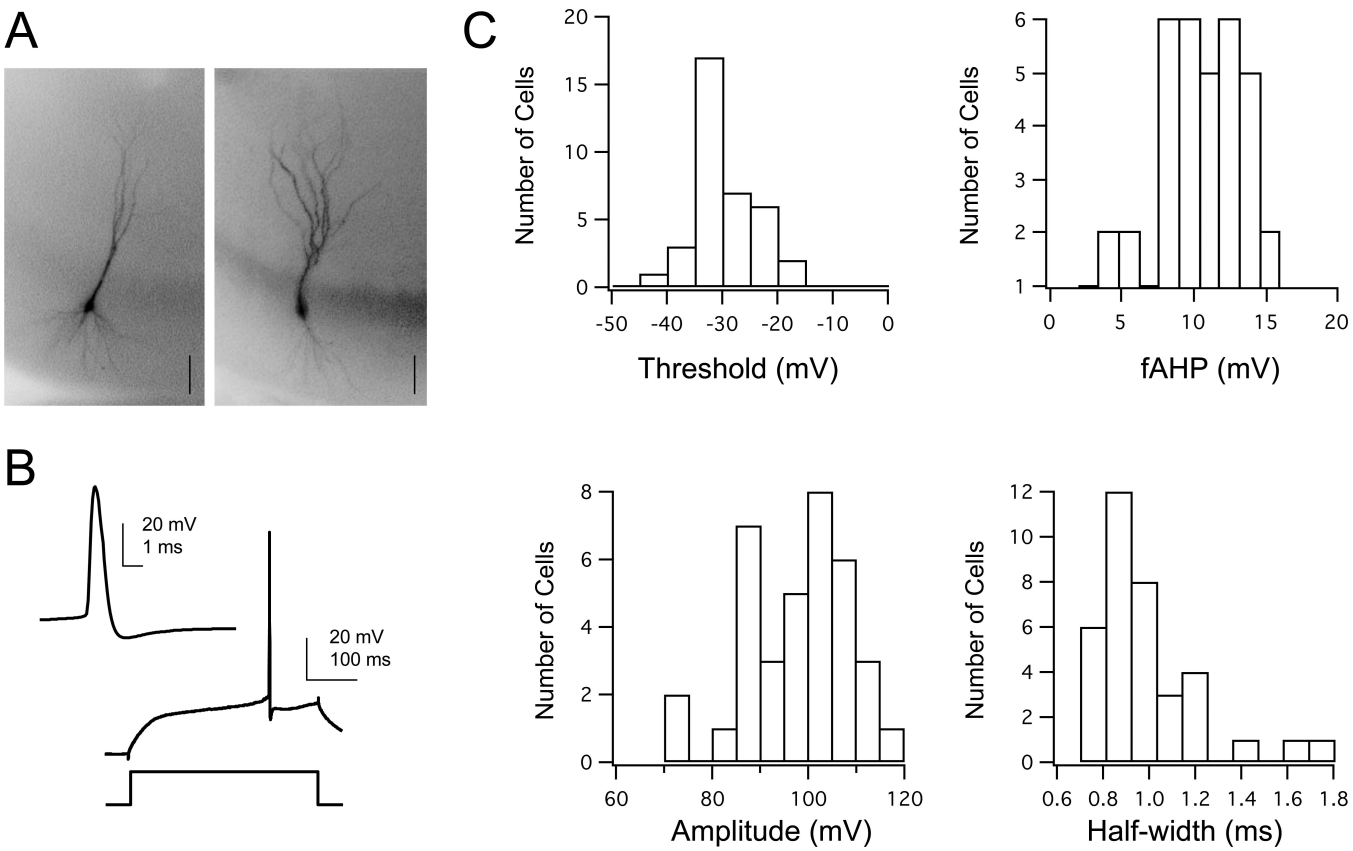

Figure 1. Characteristics of single action potentials in CA3b pyramidal neurons

A: Micrographs of CA3b pyramidal pyramidal neurons. The image on the right is the maximum projection of 10 images. Scale bars 100 μm. B: Rheobase action potential elicited by depolarizing current injection to the soma. Inset: Spike waveform shown with a smaller time scale. C: Distributions of spike threshold, amplitude, and half-width, as well as the amplitude of the fast AHP (fAHP) for rheobase current injection (n=43). Note that each of these distributions are unimodal.

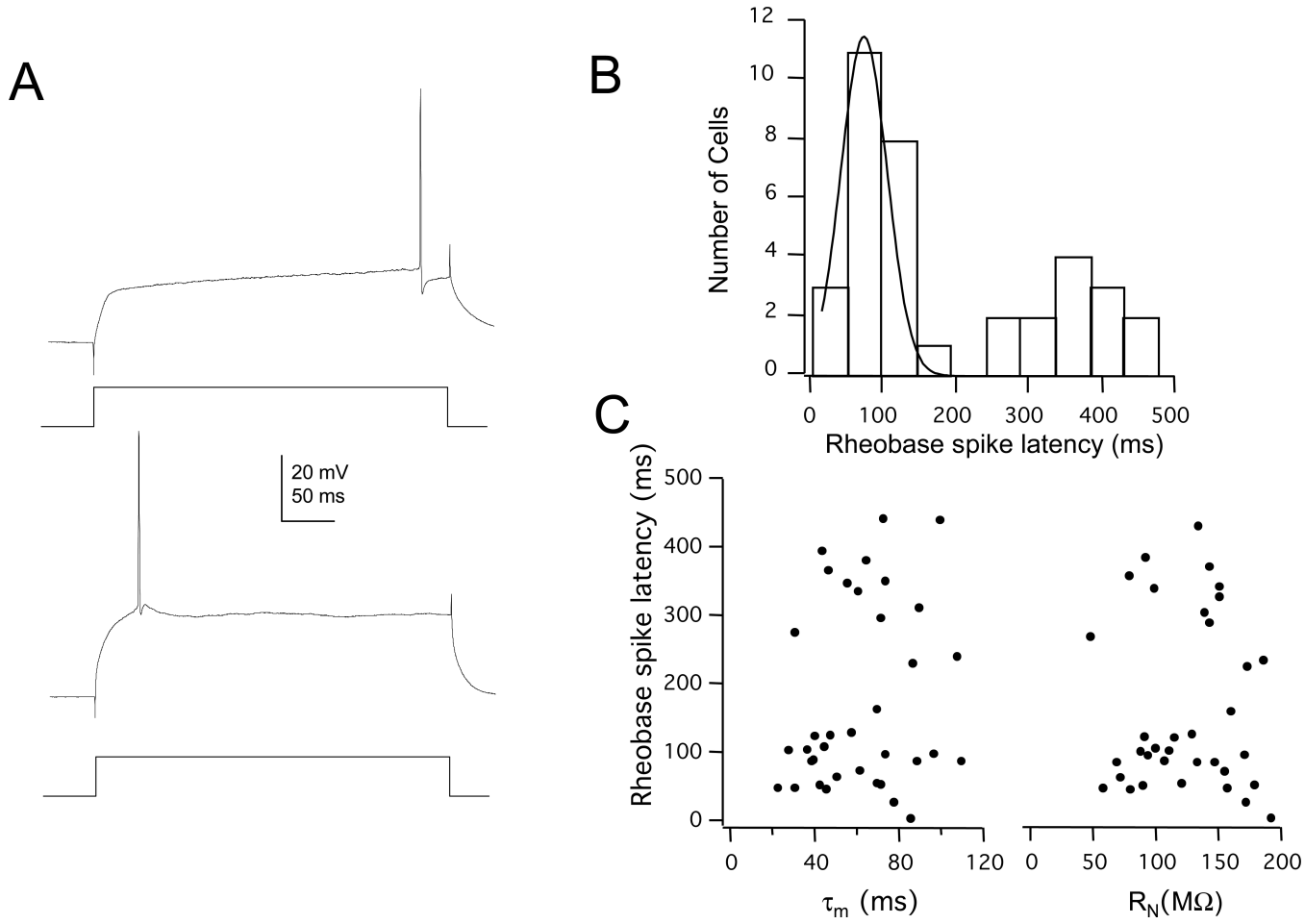

Figure 2. Early- and late-onset of rheobase spikes in CA3b pyramidal neurons

A: Representative rheobase spikes for two different cell types; late- (top) and early-onset (bottom). B: Bimodal distribution of the latency for rheobase spikes (n=43). Smooth line is a Gaussian fit to the entire data set. There was a significant difference between the smooth unimodal distribution and the distribution of experimentally-measured latencies (Kolmogorov-Smirnov test for continuous distributions, D = 0.38, n=43, $p < 0.05$). C: The bimodal distribution of spike latency was not due to a systematic difference in passive membrane properties. The membrane time constant (τ_m) and input resistance (R_N) was calculated from the slowest time constant fitted to a charging curve within -5 mV of V_{rest}. There was no significant correlation between spike latency and either of the two passive membrane parameters.

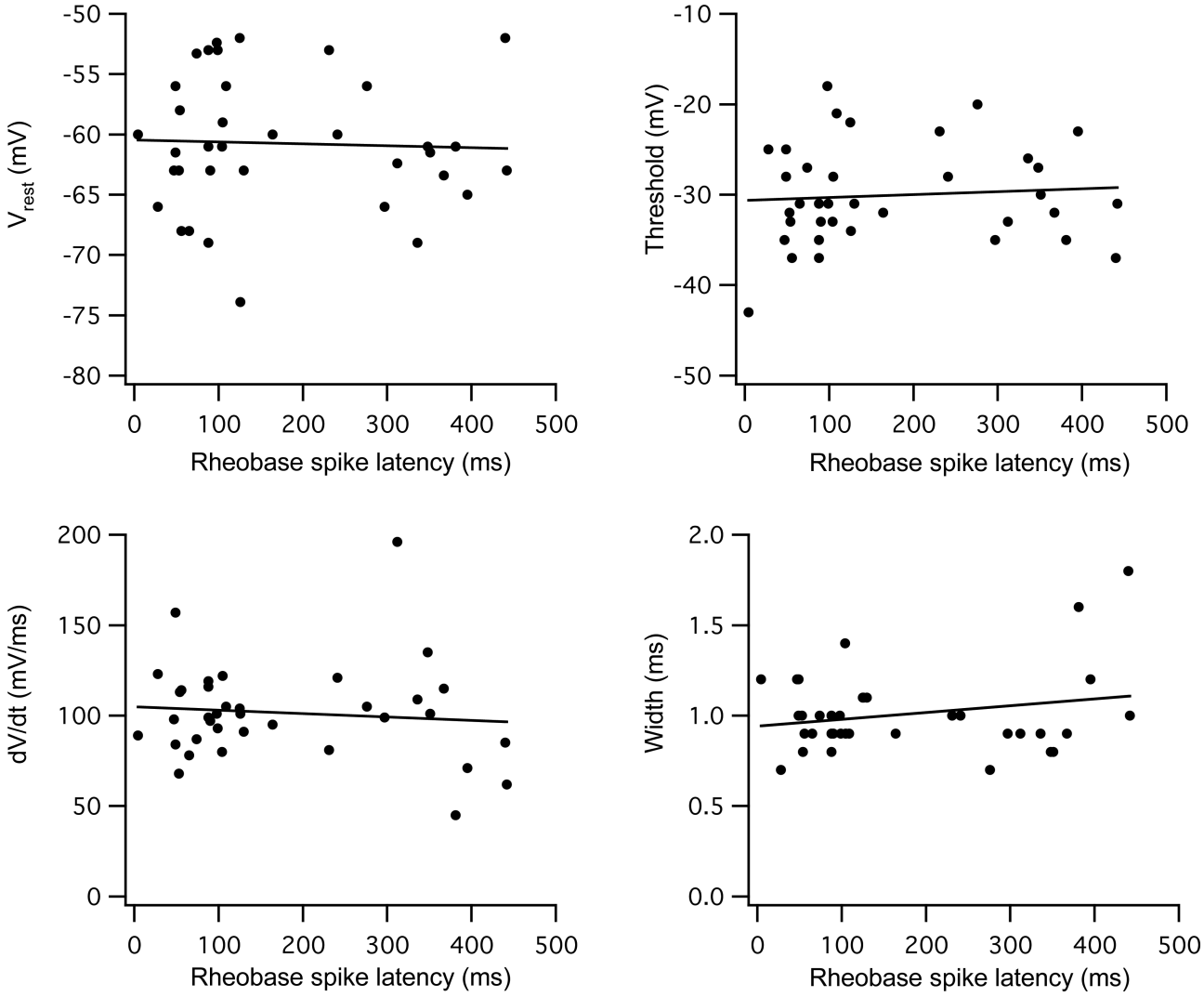

Figure 3. No correlation between cellular properties and rheobase spike latency

Resting potential and three parameters of single rheobase spikes (threshold, spike rate of rise, and half-width) are plotted against the latency for rheobase spikes. There was no significant correlation ($r^2 < 0.05$, $p > 0.05$) between these parameters and whether the cell fired with an early or late onset.

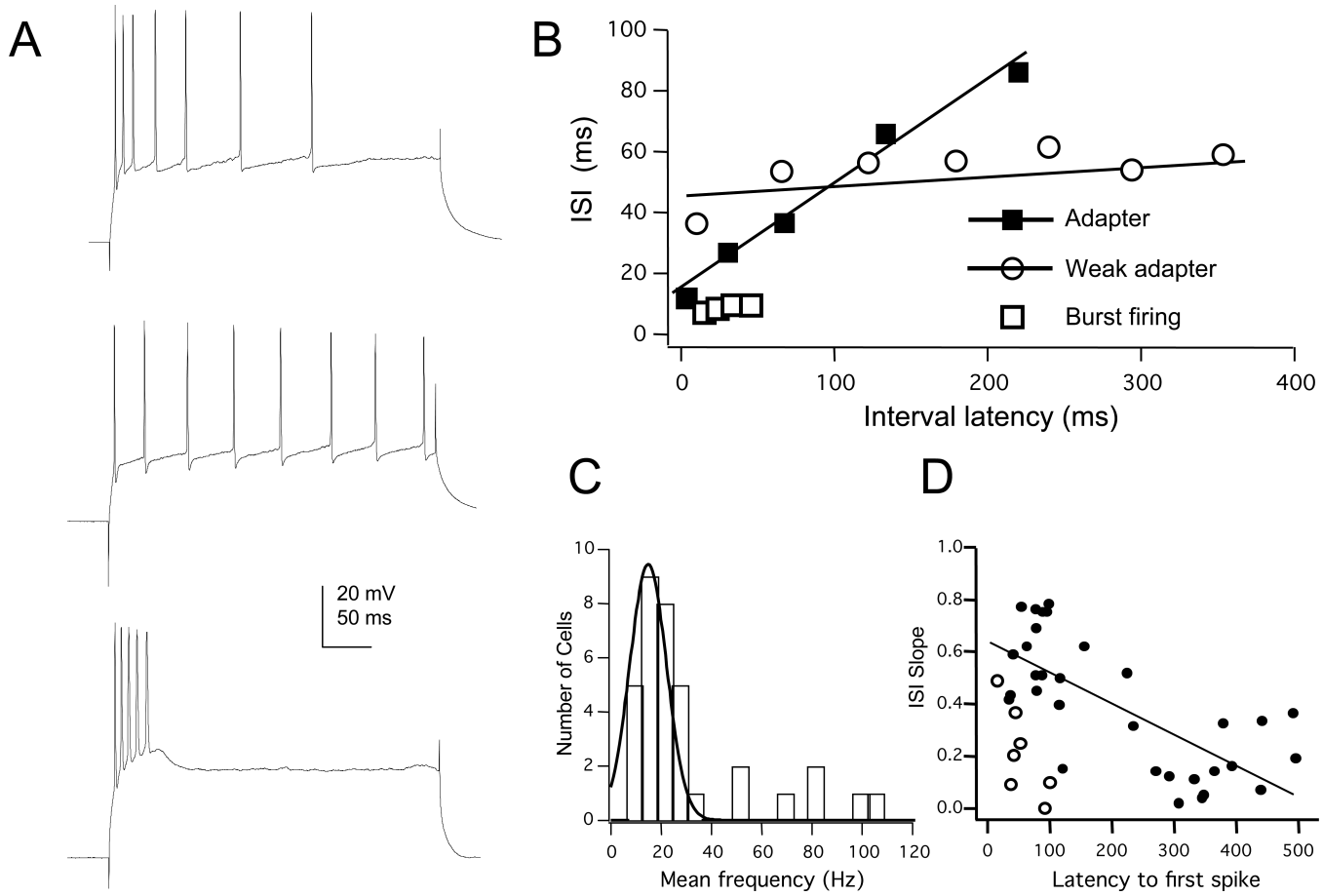

Figure 4. Three firing patterns in CA3b pyramidal neurons

A: When current amplitude was adjusted above rheobase to elicit >=4 spikes CA3b pyramidal neurons recorded in the whole-cell configuration fired either a regular, adapting train of action potentials (top trace; V_{rest} = -58 mV, R_N = 75 MΩ, τ_m = 34 ms), a train that displayed little adaptation (middle trace; V_{rest} = -63 mV, R_N = 68 MΩ, τ_m = 45 ms), or fired a high frequency burst of spikes and ceased to fire for the remainder of the depolarizing current step (bottom trace; V_{rest} = -56 mV, R_N = 57 MΩ, τ_m = 22 ms). B: Interspike interval (ISI) plots illustrating differences in spike frequency adaptation (SFA). The ISI was plotted against the latency to the second spike for each interval. The slope of this relationship was used to quantify the magnitude of SFA between cells. C: Burst-firing cells had significantly higher mean firing rates. For a train of 4 or more spikes, mean rate was 31 ± 4 ms. For a smooth Gaussian fit to the entire data set, the mean was 19 Hz. Consistent with a bimodal distribution, there was a significant difference between the unimodal distribution and the data set (Kolmogorov-Smirnov test for a continuous distribution, D=1.34, n=35, $p < 0.05$). D: The relationship of between ISI slope and the latency of rheobase spikes (see Figure 2) are plotted. Burst firing cells (open circles) were all early-onset cells and had ISI slopes that, in general, were only weakly adapting. For non-burst firing cells (filled circles), the plot illustrates the correlation between the latency of rheobase spikes with the magnitude of SFA (Pearson's correlation test, $r^2 = 0.32$, $p < 0.05$).

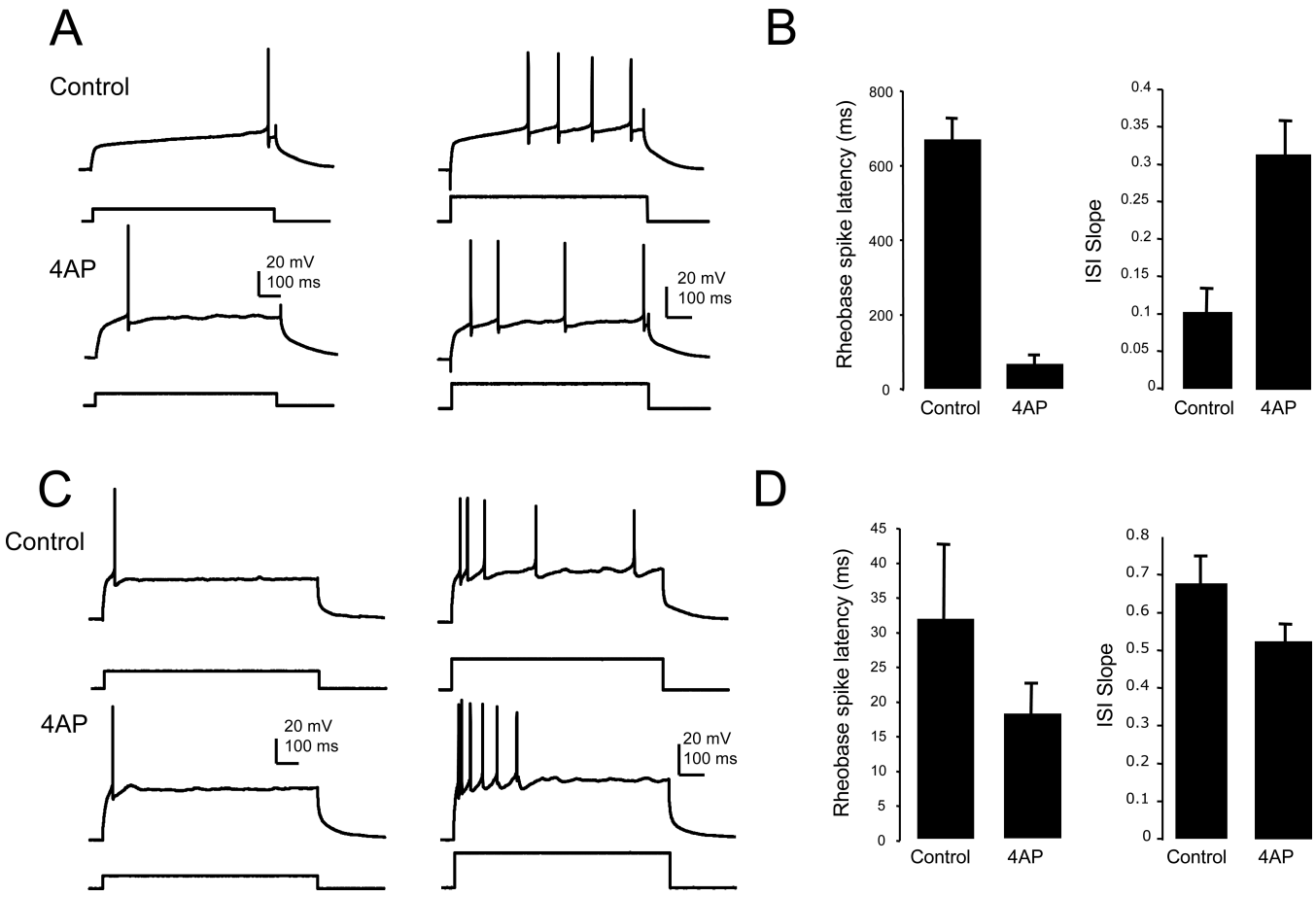

Figure 5. K^+ channel blocker 4-aminopyridine affects delayed onset, weakly adapting cells

A: For late-onset cells the bath application of a low concentration (30 μm) of 4-aminopyridine (4-AP) decreases the latency for rheobase spikes. Representative late-onset cell (V_{rest} = −63 mV, R_N=56 MΩ, τ_m = 25 ms) illustrating the effect of 4-AP on rheobase spikes (left traces) and spike trains produced by stronger current injection (right traces). B: Summary plots illustrating the effects of 30 μm 4-AP on rheobase spike latency (n=4) and ISI slope (n=3). C: Bath application of 4-AP (30 μm) had little effect on the excitability of early-onset CA3 neurons. Representative late-onset cell (V_{rest} = −66 mV, R_N=100 MΩ, τ_m = 53 ms) illustrating the effect of 4-AP on rheobase spikes (left traces) and spike trains produced by stronger current injection (right traces). D: Summary plots illustrating the effects of 4-AP on rheobase spike latency (n=3) and ISI slope for early-onset cells (n=3).

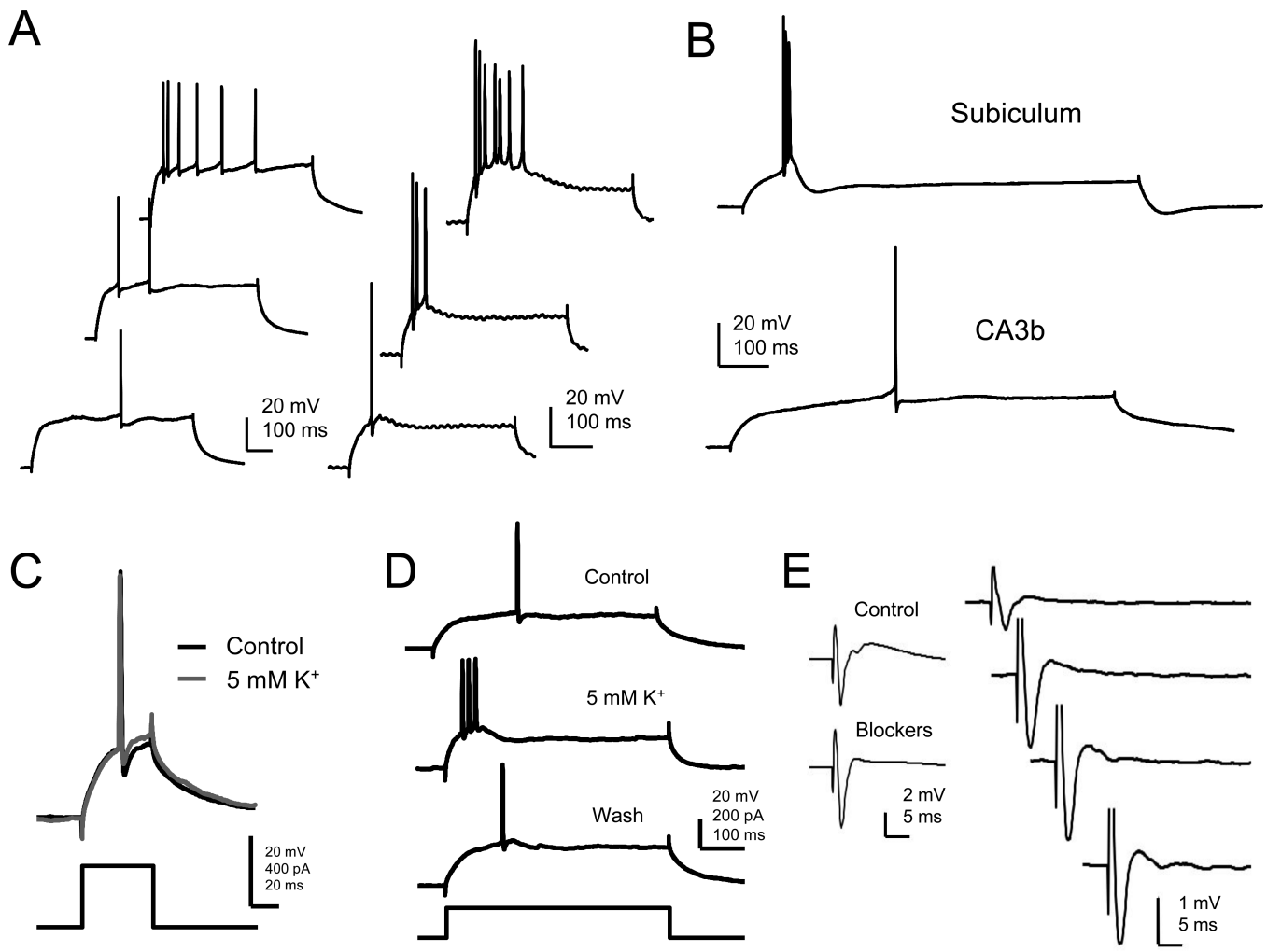

Figure 6. Burst firing in CA3b pyramidal neurons

A: Response of an adapting neuron (left traces) and a burst firing neuron (right traces) to three increasing amplitudes of depolarizing current injection. Although an afterdepolarization (ADP) is apparent for the burst firing cell (right bottom trace), it does not elicit multiple spikes. In contrast, a medium AHP (mAHP) is seen after each spike in the bottom left and middle left traces. B: *In vitro* slice conditions do not account for the low frequency of burst firing CA3b pyramidal neurons. An example of burst firing in a pyramidal neuron from the subiculum (top trace). Here a minimum amount of current injection was needed to trigger the burst. In the same slice, a minimal current injected into a CA3b pyramidal neuron triggered a single spike. C: The low occurrence of burst firing was not due to extracellular K+ concentration. Increasing K^+ to 5 mM (grey traces) from control (2.5 mM, black traces) decreased the amplitude of the fAHP in these cells but did not reveal a regenerative event or burst firing at rheobase current amplitudes. D: In contrast, with stronger and longer stimulus burst-like events could be elicited with high K^+ concentrations. E: Extracellular field potentials recorded in area CA3b in response to stimulus of the alveus. Blockers of excitatory and inhibitory synaptic transmission (see Methods) had no significant effect on the antidromic waveform (left traces). Representative example of antidromic

responses in the presence of blockers (right traces) to increasing stimulus intensities (1.15, 1.25, 1.35, & 1.45 mA; each waveform is the average of 10 traces).

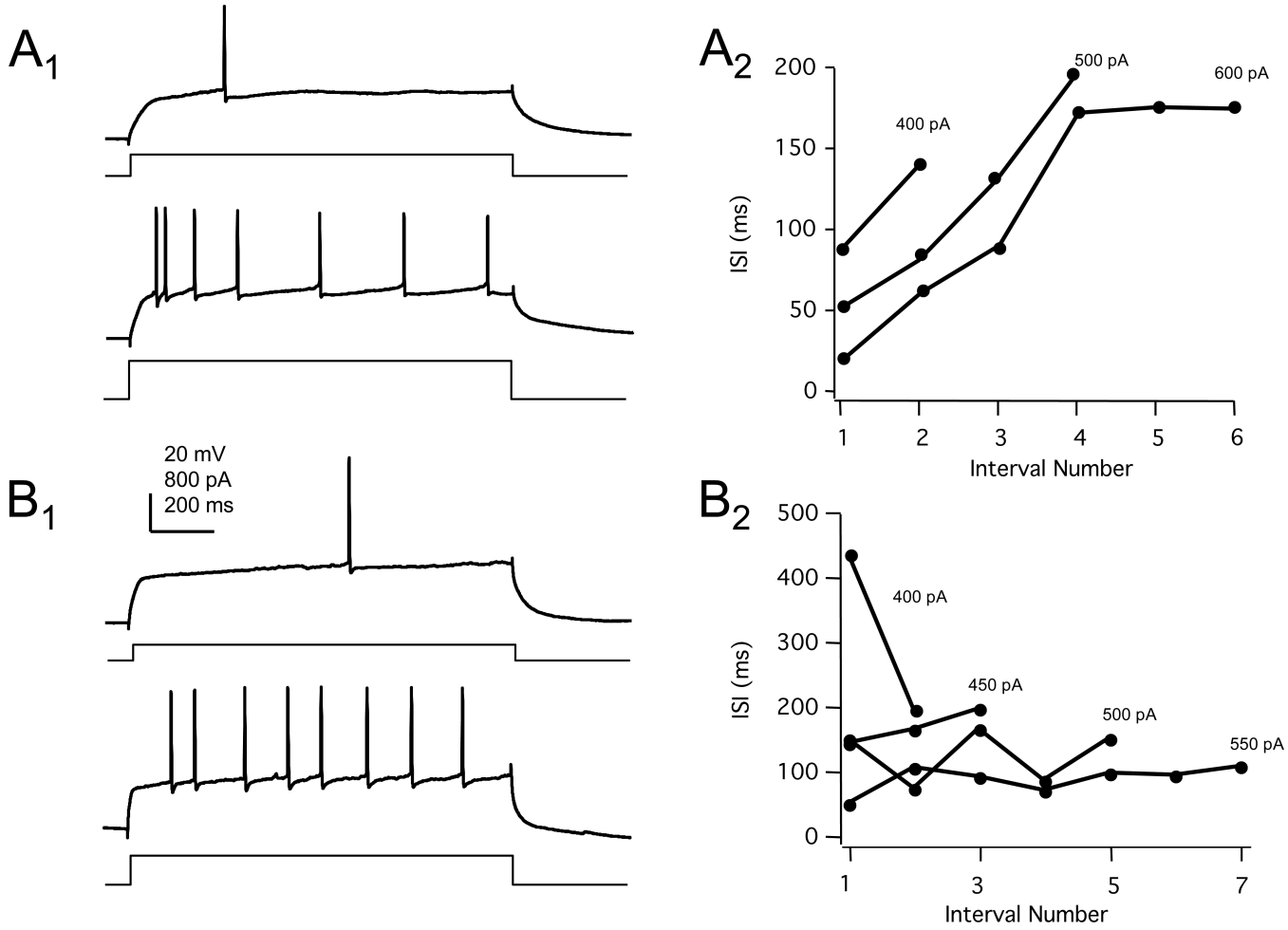

Figure 7. Perforated patch-clamp recordings of CA3b pyramidal neurons

Input/output responses from two different CA3b pyramidal neurons recorded using the nystatin patch-clamp recording method. A1: Firing of an early-onset, regular-firing neuron in response to rheobase (top traces) and stronger (bottom traces) current injection illustrating spike onset and SFA, respectively. B1: Firing of a late-onset, weakly-adapting neuron in response to rheobase (top traces) and stronger (bottom traces) current injection illustrating spike onset and weak SFA, respectively. A2 & B2: ISI plots for a range of depolarizing current injections for the two cells illustrating differences in adaptation between the neurons.

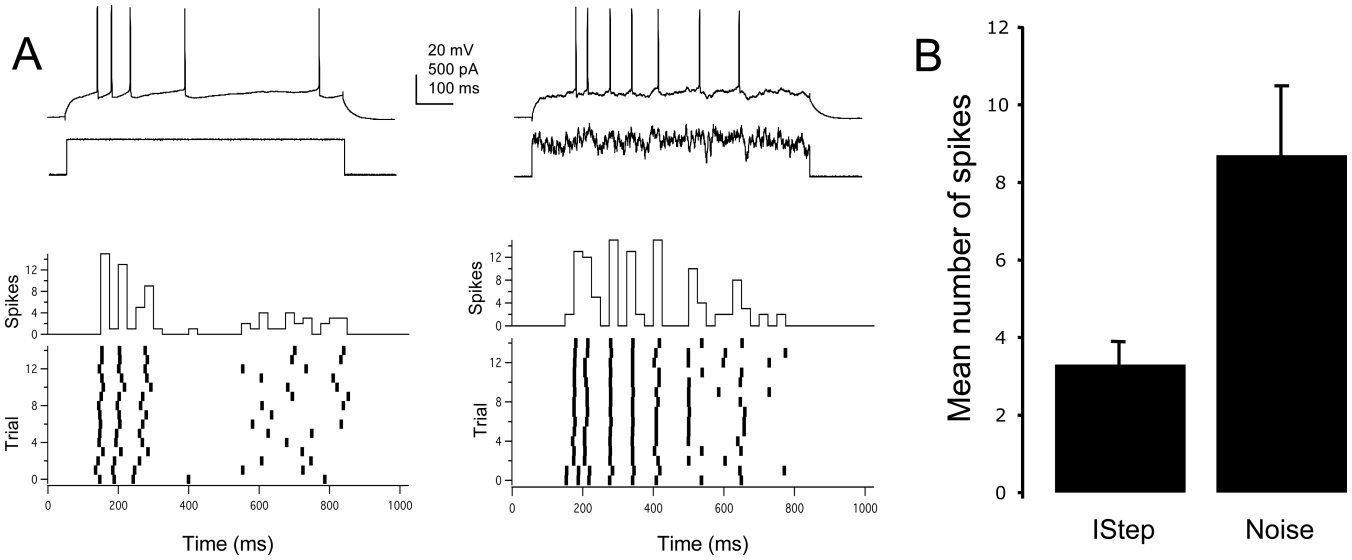

Figure 8. Firing patterns in response to simulated synaptic bombardment

A: Firing response of a CA3b pyramidal neuron in response to a rectangular depolarizing current step (left) or Poisson-like noise with the same average current (right). Raster plots of firing across sweeps (trials) and histograms of the number of spikes over discrete time domains illustrate that for a depolarizing current step firing reliability decreases over the duration of the current injection. In contrast, for the noisy input firing rate and reliability is greater. B: Summary plot illustrating the mean number of spikes per trial produced by a rectangular current step (IStep) and for current injected with “noisy” waveforms (n=10).

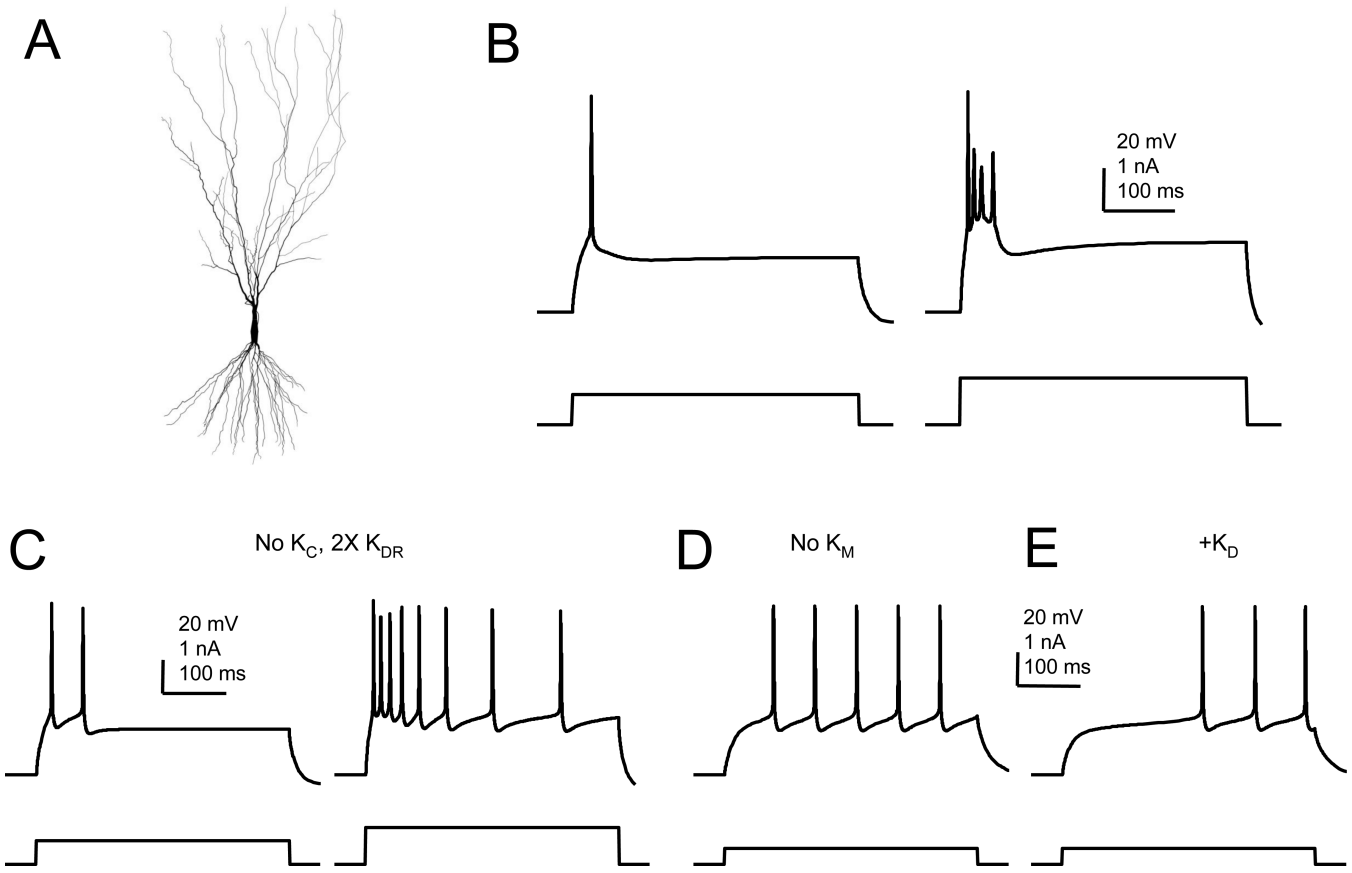

Figure 9. Models of different CA3 pyramidal neuron firing patterns

A: Reconstruction of a CA3b pyramidal neuron (*cell1zr*, Henze et al., 1996). B: Firing in response to weak and strong current intensities for a model constructed to qualitatively match the characteristics of a burst firing neuron. C: Elimination of K_C and augmentation of K_{DR} transformed the model into one that exhibited early-onset firing and strong adaptation. D: Adaptation was dependent on K_M in the model. Removal of the K_M conductance resulted in a model lacking spike frequency adaptation. E: Delayed-onset firing was achieved with the addition of a slowly-inactivating K_D conductance into the model.

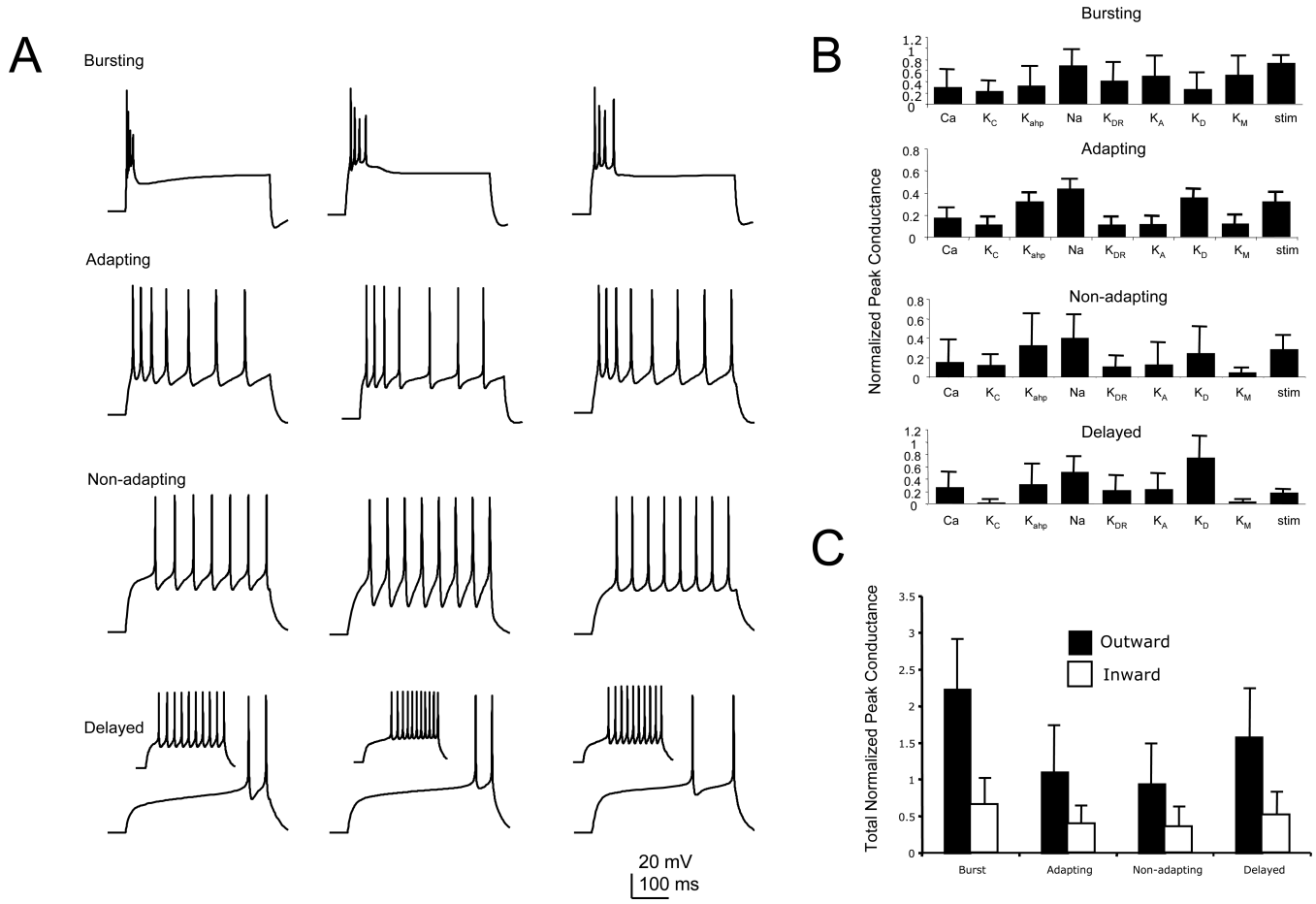

Figure 10. Exploration of parameter space in a reduced CA3 pyramidal neuron model

A: Representative examples of four types of firing patterns produced by different configurations of membrane conductances in the one compartment model. B: Normalized conductance densities (mean ± SD) for the eight channel types and the stimulus current (stim) illustrating the variability between the four firing patterns. C: The sum of the normalized outward and inward conductances are compared between the four firing patterns. Note that burst firing and delayed onset firing patterns were associated with greater outward conductances that were accompanied by larger inward conductances.